

# Remote Epitaxy of Cubic Gallium Nitride on Graphene-Covered 3C-SiC Substrates by Plasma-Assisted Molecular Beam Epitaxy

Mario Littmann,\* Dirk Reuter, and Donat Josef As\*

Remote epitaxy is a relatively new area of research that offers several advantages, including the potential to reduce the influence of lattice mismatch and the ability to exfoliate films easily. This work is focused on adapting this growth method for the epitaxy of cubic gallium nitride (c-GaN), a metastable phase. However, one faces challenges in enforcing the nucleation of the metastable cubic phase due to the weaker interactions between the substrate and the epitaxial layer compared to conventional epitaxy. Initially, only polycrystalline wurtzite gallium nitride could be grown. However, by optimizing the growth conditions and adding a cubic aluminum nitride buffer layer, predominantly cubic gallium nitride layers can be grown. High-resolution X-ray diffraction measurements confirm that the percentage of hexagonal inclusions is reduced from 80% to 23%.

## 1. Introduction

Group III nitrides are a class of semiconductor materials that are widely used in the electronics industry due to their unique physical and chemical properties.<sup>[1]</sup> For example, they have a wide bandgap, which makes them useful for optoelectronic devices such as light-emitting diodes (LEDs) and lasers, as well as for high-power electronic devices.<sup>[2,3]</sup> However, the wurtzite crystal structure of group III nitrides can lead to the quantum-confined Stark effect (QCSE), which can reduce the device efficiency. To avoid the QCSE, some researchers have explored the use of the metastable cubic GaN instead. However, growing group III nitrides is difficult because they can only be synthesized by heteroepitaxy.

One challenge of heteroepitaxy is that it is always limited by the availability of suitable substrate materials with a small lattice

mismatch. A high mismatch can lead to the formation of defects in the grown film, which can reduce the efficiency of devices based on the material. One possible solution to this is the use of remote epitaxy.<sup>[4]</sup>

The process of remote epitaxy has been an area of intense research in recent years due to its potential to overcome some of the limitations of traditional heteroepitaxy. Several studies have demonstrated the advantages this growth process provides.<sup>[5]</sup> Besides the advantage of reducing the influence of the lattice mismatch, it also allows the possibility of an easy-to-perform lift-off process. This allows either the reuse of expensive substrates or the transfer of thin epitaxial layers to host substrates in systems where no selective etching process for


releasing the layer exists, for example, the GaN/AlN system. The remote heteroepitaxy approach has been shown to be effective for various materials, including wurtzite, nitrides,<sup>[6]</sup> and arsenides,<sup>[7,8]</sup> using growth techniques such as metal-organic chemical vapor deposition (MOCVD) and molecular beam epitaxy (MBE).

In this study, we report on the successful adaption of the remote epitaxy process for the cubic zinc blende gallium nitride (c-GaN), which is a novel application of this process to grow a metastable phase. Cubic GaN has typically been grown on (001) zinc blende silicon carbide (3C-SiC), which has the smallest possible lattice mismatch of 3.2%. This mismatch is still high enough to result in the formation of a large number of defects in the grown film. To address this problem, we explored the use of remote epitaxy, using a thin layer of the 2D material graphene as an intermediary layer between the substrate and the epitaxial layer. The use of the 2D material allows for a significant reduction in interactions between the substrate and the epitaxial layer, as the graphene is only bonded to the substrate by van-der-Waals forces rather than covalent bonds. This may help to reduce the formation of defects in the grown film, improving the efficiency of devices based on c-GaN.<sup>[4,5]</sup>

## 2. Experimental Section

In a first step, a single layer of graphene was transferred onto the substrate material. We used a 3C-SiC/Si (001) pseudosubstrate from the company NovaSiC. The substrate consisted of a 10  $\mu\text{m}$  3C-SiC layer on top of a 500  $\mu\text{m}$  silicon (001) wafer. To cover them with a graphene monolayer, we used the

M. Littmann, D. Reuter, D. J. As  
Department of Physics  
Paderborn University  
Warburger Straße 100, 33098 Paderborn, Germany  
E-mail: mariolit@mail.uni-paderborn.de; d.as@uni-paderborn.de

 The ORCID identification number(s) for the author(s) of this article can be found under <https://doi.org/10.1002/pssb.202300034>.

© 2023 The Authors. physica status solidi (b) basic solid state physics published by Wiley-VCH GmbH. This is an open access article under the terms of the Creative Commons Attribution License, which permits use, distribution and reproduction in any medium, provided the original work is properly cited.

DOI: 10.1002/pssb.202300034

“Trivial Transfer” graphene from the company ACSMaterial. This graphene was created by a CVD process on copper foils.<sup>[9]</sup> The graphene was delivered on a polymer and covered with a polymethyl methacrylate (PMMA) photoresist. To separate the graphene from the polymer, it can be placed in water. The photoresist-covered graphene will float on the surface while the polymer sinks to the bottom.

The new target substrate could be used to pick the graphene out of the water. Afterward, the sample must naturally dry for 30 min and then be baked for 20 min at 100 °C on a hotplate. The last step was to remove the photoresist. The 500 nm-thick photoresist can be mostly removed by immersing the sample into 50 °C hot acetone. However, small micrometer-sized photoresist residues remained on the sample surface (Figure 1a). The work of Pirkle et al.<sup>[10]</sup> suggests a thermal vacuum annealing step to remove the residues. Therefore, we performed a second thermal cleaning step. By heating the sample to 900 °C for 15 min in a vacuum chamber, we were able to remove the photoresist completely. The result is shown in Figure 1b. The sample was ready for the epitaxy after this.

It is worth noting that the scanning electron microscope (SEM) images of the graphene in Figure 1b showed dark lines corresponding to domain boundaries, which matched the description of the nucleation process of the graphene CVD process provided by Xiang et al.<sup>[11]</sup> The average domain size of our samples was about 1 μm in diameter. In comparison, the average size of antiboundary domains (ABD) in the used 3C-SiC substrates was ten times larger.<sup>[12]</sup> According to the manufacturer, the thickness of the graphene was guaranteed to be one monolayer. We confirmed this using Raman spectroscopy measurements after the transfer, which showed compliance with the characteristics of monolayer graphene,<sup>[13]</sup> including the presence of a G peak at  $\approx 1580 \text{ cm}^{-1}$  and a 2D peak at  $2680 \text{ cm}^{-1}$ .

The epitaxy of GaN in this work was performed with a plasma-assisted MBE (PAMBE). A gallium flux of  $3.6 \times 10^{14} \text{ atoms [cm}^2 \text{ s]}^{-1}$  was used for every sample. The nitrogen plasma source was operated with a radio-frequency (RF) power of 260 W and an N<sub>2</sub> flux of 0.5 sccm. These conditions corresponded to a growth velocity of  $150 \text{ nm h}^{-1}$  or  $0.4 \text{ Å s}^{-1}$  for our standard growth conditions on the pure 3C-SiC substrate.<sup>[14]</sup>

Postgrowth characterization of the surface was done with SEM and atomic force microscopy (AFM). In addition, we used

high-resolution X-ray diffraction (HRXRD) and photoluminescence (PL) measurements to analyze the crystal quality and phase.

The PL measurements were performed with an Nd:YAG laser with a wavelength of 266 nm and a power of 5 mW. The samples were mounted inside a cryostat to cool them down to a temperature of 13 K.

### 3. Results

We started by growing c-GaN under standard conditions used on pure 3C-SiC substrates with a substrate temperature of 745 °C. Even though we could grow GaN, the grown films were polycrystalline and hexagonal. While other publications<sup>[5]</sup> about remote epitaxy suggest a better result by starting the growth under colder conditions, we observed that this method only enhanced the formation of the hexagonal phase. Figure 2a shows an SEM image of the surface of the resulting polycrystalline GaN layer. Due to the fact that the lower substrate temperature enhances the nucleation probability too strongly, the atoms no longer align themselves with the underlying crystal structure. Noteworthy is the fact that the nucleation around the graphene domain boundaries seems to be enhanced. In comparison, the areas between the domain boundaries show a more uniform growth. However, after a longer growth time, these areas also turn hexagonal and polycrystalline (see Figure 2b).

We used HRXRD measurements to analyze the crystal orientations. In Figure 3a, the reciprocal space map (RSM) of the symmetrical (002) reflection is shown for the sample shown in Figure 2b. As described by Frentrup et al.,<sup>[15]</sup> the area around the (002) reflection is not only containing the (0002) reflection of the wurtzite and cubic GaN but also the (10-11) and (-1011) reflections originating from wurtzite GaN. The last two reflections correspond to the wurtzite GaN grown on top of the (111) facets of the zinc blende crystal. This allows for an easy comparison of the different phase compositions inside the epitaxial layer. The most intense GaN reflection of the map in Figure 3a is the (0002) reflection corresponding to the hexagonal phase. By comparing the intensities of the reflections, we can conclude that the epitaxial layer consists of 80% wurtzite GaN, which is consistent with the conclusions from the SEM image in Figure 2b. Every sample was measured two times by rotating

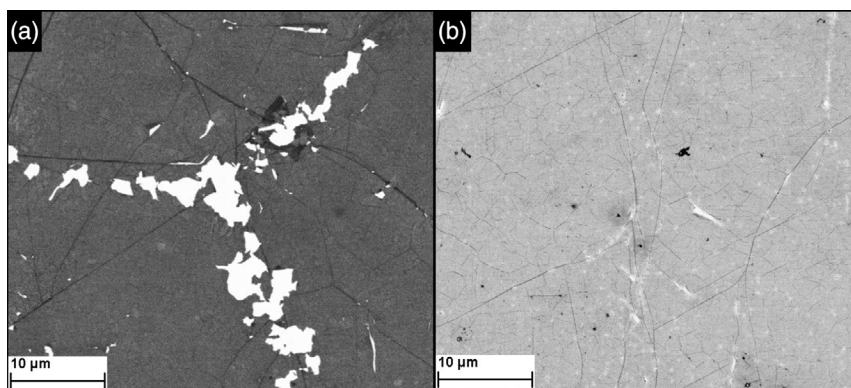


**Figure 1.** SEM images of the surface of a 3C-SiC/Si sample covered with graphene. a) After the acetone cleaning step with the visible PMMA residues. b) After the thermal vacuum annealing step (900 °C for 15 min).

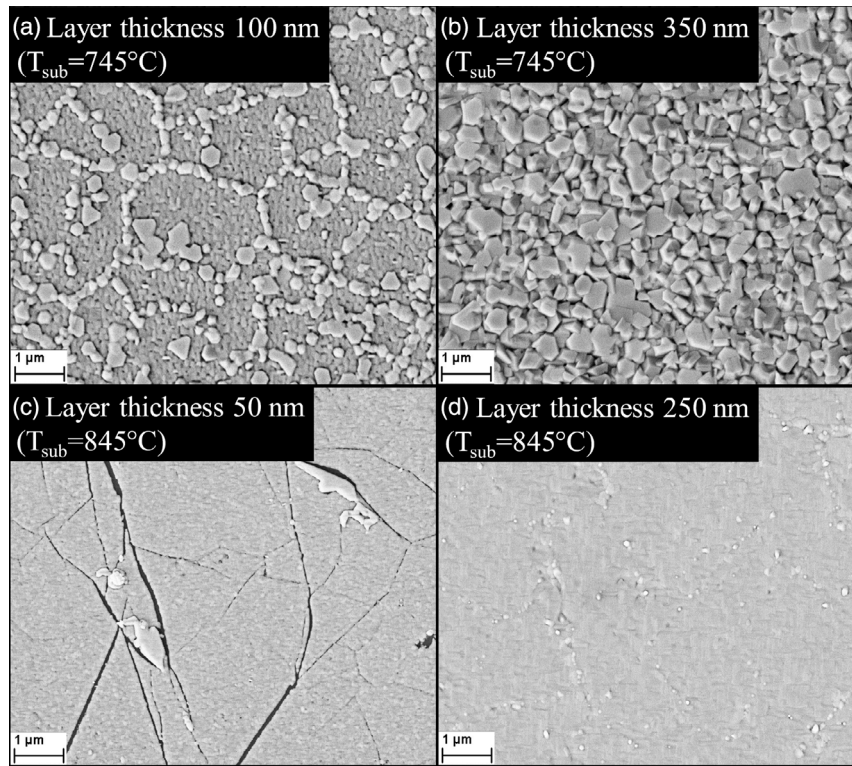


**Figure 2.** SEM images of the surface of several 3C-SiC samples covered with graphene and overgrown with GaN: a) GaN layer grown on top of a graphene layer ( $T_{\text{sub}} = 745^\circ\text{C}$ ). b) Thicker GaN ( $T_{\text{sub}} = 745^\circ\text{C}$ ). c) Thin GaN layer grown ( $T_{\text{sub}} = 840^\circ\text{C}$ ). d) Thicker GaN layer ( $T_{\text{sub}} = 840^\circ\text{C}$ ).

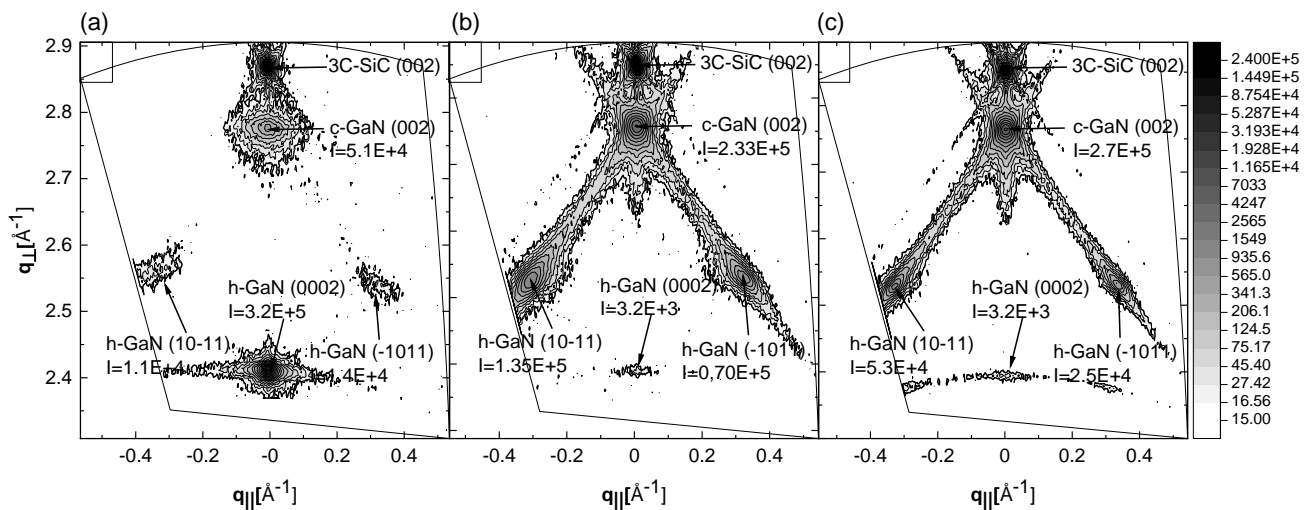


**Figure 3.** RSM containing the cubic (002) and the hexagonal (0002), (10-11), and (-10-11) reflections of three samples grown on a graphene monolayer: a) 350 nm-thick GaN grown on a 3C-SiC/Si substrate at  $T_{\text{sub}} = 745^\circ\text{C}$  (SEM, see Figure 2b). b) 260 nm-thick GaN grown on a 3C-SiC/Si substrate at  $T_{\text{sub}} = 840^\circ\text{C}$  (SEM, see Figure 2d). c) 300 nm-thick GaN grown on a thin c-AlN buffer layer at  $T_{\text{sub}} = 845^\circ\text{C}$  (SEM, see Figure 5b).

the sample by  $90^\circ$ . This high amount of hexagonal inclusions is primarily caused by the changed growth condition due to the introduction of the graphene monolayer. It is possible to grow phase-pure c-GaN with less than 1% hexagonal inclusions directly on the 3C-SiC substrate under these conditions.

This means that for the remote epitaxy of a metastable phase like zinc blende GaN, it is not possible to use a low-temperature buffer layer. On the contrary, the opposite is the case. By increasing the substrate temperature to about  $845^\circ\text{C}$ , we could grow partial cubic GaN. The used temperature is only  $10^\circ\text{C}$  under the



maximal possible growth temperature since our experiments showed no nucleation at a substrate temperature over 855 °C.

Figure 2c,d shows the SEM images of two samples grown with a substrate temperature of 845 °C. Two main improvements in the quality are visible. First, nucleation along the domain boundaries seems to be suppressed under these conditions. Figure 2c shows gaps inside the layer which run along the domain boundaries. The second improvement is the fact that the surface is more homogeneous and only contains slight polycrystalline inclusions. AFM measurements confirm a smooth surface with a root mean square (RMS) roughness of 5 nm.

Furthermore, the HRXRD results show a significant reduction of the (0002) phase (Figure 3b), and the RSM shows an increased intensity at the (10-11) and (-1011) reflections. These reflections also correspond to the hexagonal phase. However, they only form on the (111) facets of the cubic crystal. By comparing the intensities of the reflections, it can be concluded that the GaN layers are composed of 60% cubic phase. Therefore, we were able to grow a predominant cubic GaN layer.

These results demonstrate that the growth at lower temperatures leads to direct nucleation in the hexagonal (0002) phase. In contrast, increasing the substrate temperature during growth helps to increase the formation of the cubic (002) phase. This correlation is believed to be due to the reduced nucleation probability at higher temperatures, which enhances the interaction with the dangling bonds of the underlying substrate. Notably, only layers grown with low nucleation probability showed alignment with the substrate crystal structure. The results highlight the importance of controlling nucleation in the remote epitaxy process.

However, the amount of hexagonal inclusions is significantly too high for device applications, and further optimizations of the growth process are necessary. It can be concluded that a solution is needed to increase the influence of the substrate material underneath the graphene layer to foster the nucleation of cubic GaN. It can be expected that the influence of the dangling bonds of the substrate surface depends on the chemical polarity of the atomic bonds in the crystal.<sup>[16]</sup> In the case of 3C-SiC, the difference in the electronegativity values is 0.76.<sup>[17]</sup> Since silicon and carbon are both in the fourth group of the periodic table, this is a relatively small value. By introducing an additional thin buffer layer underneath the graphene, it is possible to increase the chemical polarity. The PAMBE used in this study also contains an aluminum cell, which allows for the growth of a cubic aluminum nitride layer (c-AlN). In comparison, the difference in electronegativity is with a value of 1.45, significantly higher than for 3C-SiC. Furthermore, the lattice mismatch of c-AlN to 3C-SiC is only 0.3%,<sup>[18]</sup> which allows the growth of a low-defect layer.

New samples were prepared with an AlN buffer layer below the graphene layer to investigate this. The cubic AlN layer was grown with an Al flux of  $1.4 \times 10^{14}$  atoms [cm<sup>2</sup>s]<sup>-1</sup> and had a thickness of  $\approx 10$  nm, which was confirmed by X-ray reflection measurements. This is below the critical thickness, that is, the AlN layer should have grown pseudomorphically and, therefore, should have low defect density. After the AlN buffer growth, the samples were again covered with a monolayer of graphene in the same procedure as described before.

A sample series with different growth durations were grown to further analyze the growth procedure. Figure 4 shows results for

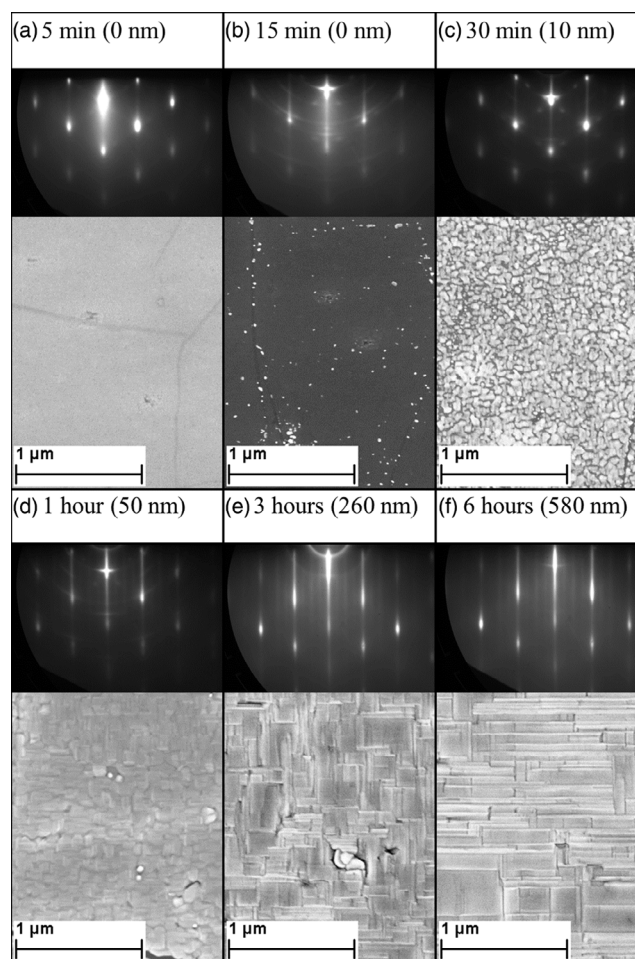


**Figure 4.** RHEED pattern and SEM images of a sample series with different growth durations from a) 5 min to f) 6 h. The samples were all grown on a c-AlN buffer layer with a substrate temperature of 845 °C.

the sample series with different growth times from 5 min to 6 h. The figure contains the reflection high-energy electron diffraction (RHEED) pattern at the end of each growth and an SEM image of the surface. The SEM images show delayed nucleation in the first minutes of the deposition. After the first 5 min (see Figure 4a), the graphene layer is still uncovered, which indicates that GaN does not nucleate. Ten minutes later (see Figure 4b), small dots form. However, these islands only cover a small part of the surface area. It takes another 15 min (see Figure 4c) for GaN to cover the graphene layer completely. The RHEED pattern at the beginning also shows a point pattern, which consistently indicates a 3D surface morphology.<sup>[19]</sup> The most significant change in the characteristics happens in the second half of the first hour (see Figure 4d). The RHEED pattern transitions from the 3D point pattern to the 2D line pattern. This is consistent with the SEM image, which also shows a more uniform layer. Further growth results in an additional qualitative improvement. The dots of the RHEED pattern further transform into a distinct line pattern, and the surface morphology changes into a smooth layer with cubic facets (see Figure 4e,f).

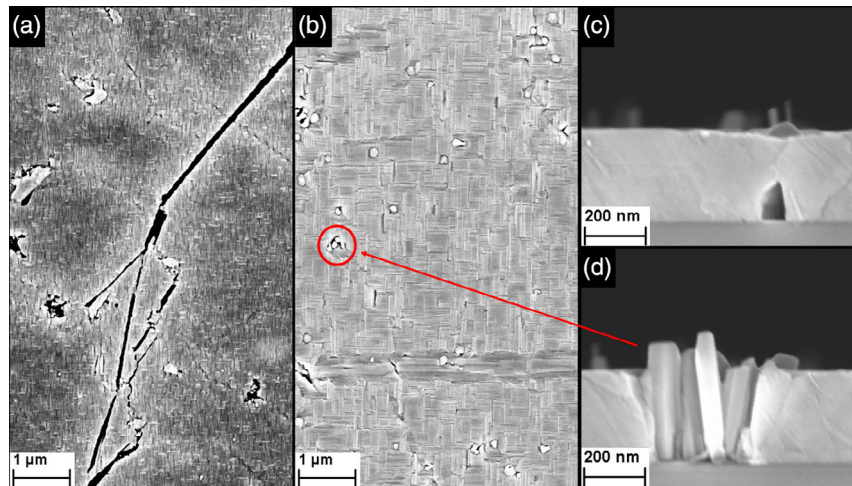


**Figure 5.** SEM images of GaN layers grown on top of a graphene-covered AlN buffer layer: a) 50 nm-thick GaN layer with visible gaps caused by the graphene domain boundaries; b) 300 nm-thick GaN layer; c) side view of an overgrown domain boundary; and d) side view of a polycrystalline defect indicated exemplarily by the red circle in (b).

Even though the samples show a uniform and smooth layer surface, this is only the case for small areas. AFM measurements in a small defect-free  $5\ \mu\text{m}$ -large square confirm an RMS roughness of 3 nm for the 260 nm sample (SEM, see Figure 4e) and 4 nm for the 580 nm sample (SEM, see Figure 4f). These values are comparable to c-GaN layer grown without graphene. Due to the characteristics of the CVD graphene layer, different defects are included in the layer. First, the nucleation under the used conditions is prevented along the domain boundaries of the graphene layer. This results in the formation of gaps throughout the layer, as shown in Figure 5a. However, these are only visible up to a layer thickness of 100 nm. After a longer growth duration, these gaps begin to become overgrown from the sides.

An example of this is shown in the cross-section SEM image in Figure 5c. The second kind of defect is the formation of small polycrystalline inclusions. These tiny dots are visible in Figure 5b). These are suspected of forming on top of the graphene monolayer defects. Due to the transfer process, it is impossible to prevent the thin film from being damaged. A cross-section image of these defects is shown in Figure 5d. The density of these defect points is about  $10^7\ \text{cm}^{-2}$ .

To prevent these defects from forming, it would be necessary to use a different process for graphene preparation without the transfer step. A possible second method for future experiments could be the thermal decomposition of SiC. The work of Ouerghi et al.<sup>[20]</sup> confirms that this is possible for 3C-SiC (100). By heating the SiC to a high temperature of 1300 °C in a vacuum, the surface silicon atoms will sublime, and the remaining carbon atoms will form a graphene monolayer. This would result in the best possible quality graphene. However, in this case, it is no longer possible to use the AlN buffer layer, which showed a significant improvement in the layer quality. Another method could be the epitaxial growth of the graphene monolayer directly on top of the cubic AlN layer.<sup>[21]</sup> This method may produce lower-quality graphene than the thermal decomposition. But it can still eliminate the defects from the transfer process, which may be the most

significant ones. Furthermore, this method still provides the possibility to use the AlN layer to reduce the hexagonal inclusions.

Furthermore, the samples grown on a c-AlN buffer layer were also characterized by HRXRD and PL measurements. The RSM shown in Figure 3c indicates a reduction of the hexagonal inclusions to about 23%. Compared to the 40% without the AlN buffer layer, it can be concluded that the buffer layer had the anticipated effect. Compared to Figure 3b, the intensities have shifted further from the facets to the (002) reflection.

Alongside the HRXRD measurements, PL measurements can be performed to gain information about phase composition. This is because the difference in the crystal phase also affects the bandgap energy. For example, the bandgap energy of wurtzite GaN at 0 K is 3.47 eV,<sup>[22]</sup> which is higher than the bandgap of zinc blende GaN with a bandgap energy of 3.293 eV.<sup>[23]</sup> This makes it possible to compare the luminescence caused by the different phases. Furthermore, the penetration depth of the used laser is only about 100 nm.<sup>[23]</sup> The PL measurements can therefore be used to obtain information about the surface area of the layer.

Figure 6 shows the PL spectra of three different samples with increasing sample thickness. Besides the different growth times, the samples were grown under the same conditions on a graphene/c-AlN substrate. Consistent with the HRXRD measurement, the spectra show a higher intensity for the cubic excitonic peak (X). Furthermore, the cubic-to-hexagonal intensity ratio increases with the film thickness. Considering the penetration depth, it can be concluded that the formation of the hexagonal phase occurs mainly at the beginning of the growth, that is, the nucleation phase. This coincides with the previous observations in Figure 4. Since the growth at the beginning is 3D, the possibility of nucleation on the (111) facets is increased, which results in the formation of hexagonal inclusions. This conclusion is additionally supported by the high intensity corresponding to the basal stacking faults (BSF)<sup>[24]</sup> at an energy of about 3.42 eV.

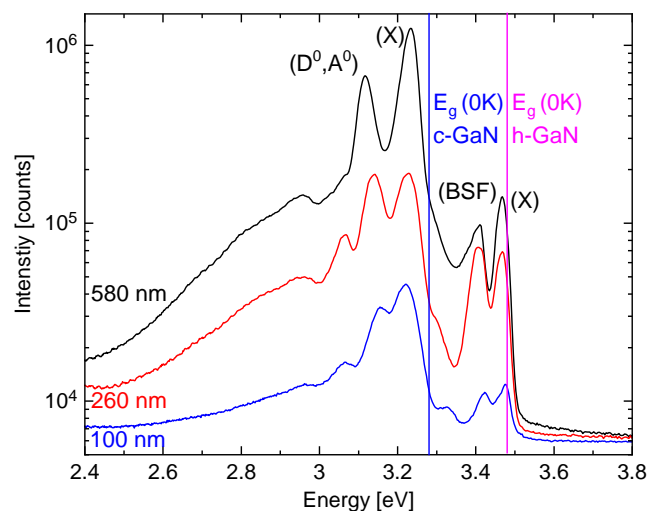


**Figure 6.** PL spectra of three GaN layers grown on an AlN buffer layer with different thicknesses. The measurements were performed at 13 K. The peaks correspond to the donor–acceptor transition ( $D^0, A^0$ ), the excitation transition (X), and the BSF.

## 4. Conclusion

In summary, we reported on the remote epitaxy of a metastable material system, zinc blende GaN, on transfer graphene-covered substrates. The transfer process was successfully performed, and with the adjusted thermal cleaning process, we were able to remove the PMMA residues from the graphene layer completely. Furthermore, we investigated different growth conditions. In contrast to previous works on remote epitaxy on other material systems, we observed that it is essential to increase the substrate temperature rather than decrease it. This resulted in the formation of the desired cubic phase. However, for the growth on graphene-covered 3C-SiC/Si (001) substrates, we were only able to grow 60% phase pure cubic GaN. A further reduction of the hexagonal inclusion was possible by increasing the chemical polarity of the used substrate material. To achieve this, we added an additional c-AlN buffer layer underneath the graphene. This step resulted in a further reduction of the hexagonal inclusions to 23%.

Two factors currently limit the quality of the GaN layer. First, the initial formation of islands at the beginning of the growth increases the hexagonal formations on the (111) facets of the cubic crystal. The second factor is the quality of the used graphene transfer process, which introduces many defects in the epitaxial layer. To improve the graphene quality, we suggest two alternative methods. The first method could be the graphitization of the 3C-SiC substrate. The second method would be the epitaxial growth with a carbon effusion cell directly on top of the c-AlN.

## Acknowledgements

The authors gratefully acknowledge the group of Rüdiger Goldhahn and Elias Kluth for the Raman spectroscopy measurements of the graphene-covered substrate material. This work was financially supported by the Deutsche Forschungsgemeinschaft (DFG, German Research

Foundation) and the transregional collaborative research center TRR 142 project B02 project number 231447078.

Open Access funding enabled and organized by Projekt DEAL.

## Conflict of Interest

The authors declare no conflict of interest.

## Data Availability Statement

The data that support the findings of this study are available from the corresponding author upon reasonable request.

## Keywords

gallium nitride, graphene, molecular beam epitaxy, remote epitaxy, zinc blende

Received: January 23, 2023

Revised: March 2, 2023

Published online: April 7, 2023

- [1] S. Strite, *J. Vac. Sci. Technol. B* **1992**, *10*, 1237.
- [2] B. J. Baliga, *Semicond. Sci. Technol.* **2013**, *28*, 074011.
- [3] S. Nakamura, M. R. Krames, *Proc. IEEE* **2013**, *101*, 2211.
- [4] T. Journot, H. Okuno, N. Mollard, A. Michon, R. Dagher, P. Gergaud, J. Dijon, A. V. Kolobov, B. Hyot, *Nanotechnology* **2019**, *30*, 505603.
- [5] J. Kim, C. Bayram, H. Park, C.-W. Cheng, C. Dimitrakopoulos, J. A. Ott, K. B. Reuter, S. W. Bedell, D. K. Sadana, *Nat. Commun.* **2014**, *5*, 4836.
- [6] A. Koma, *Thin Solid Films* **1992**, *216*, 72.
- [7] T. Henksmeier, J. F. Schulz, E. Kluth, M. Feneberg, R. Goldhahn, A. M. Sanchez, M. Voigt, G. Grundmeier, D. Reuter, *J. Cryst. Growth* **2022**, *593*, 126756.
- [8] Y. Kim, S. S. Cruz, K. Lee, B. O. Alawode, C. Choi, Y. Song, J. M. Johnson, C. Heidelberger, W. Kong, S. Choi, K. Qiao, I. Almansouri, E. A. Fitzgerald, J. Kong, A. M. Kolpak, J. Hwang, J. Kim, *Nature* **2017**, *544*, 340.
- [9] X. Li, W. Cai, J. An, S. Kim, J. Nah, D. Yang, R. Piner, A. Velamakanni, I. Jung, E. Tutuc, S. K. Banerjee, L. Colombo, R. S. Ruoff, *Science* **2009**, *324*, 1312.
- [10] A. Pirkle, J. Chan, A. Venugopal, D. Hinojos, C. W. Magnuson, S. McDonnell, L. Colombo, E. M. Vogel, R. S. Ruoff, R. M. Wallace, *Appl. Phys. Lett.* **2011**, *99*, 122108.
- [11] Y. Xiang, S. Xie, Z. Lu, X. Wen, J. Shi, M. Washington, G.-C. Wang, T.-M. Lu, *J. Appl. Phys.* **2021**, *130*, 065301.
- [12] R. Maria Kemper, T. Schupp, M. Häberlen, T. Niendorf, H.-J. Maier, A. Dempewolf, F. Bertram, J. Christen, R. Kirste, A. Hoffmann, J. Lindner, D. Josef As, *J. Appl. Phys.* **2011**, *110*, 123512.
- [13] A. C. Ferrari, J. C. Meyer, V. Scardaci, C. Casiraghi, M. Lazzeri, F. Mauri, S. Piscanec, D. Jiang, K. S. Novoselov, S. Roth, A. K. Geim, *Phys. Rev. Lett.* **2006**, *97*, 187401.
- [14] J. Schörmann, S. Potthast, D. J. As, K. Lischka, *Appl. Phys. Lett.* **2007**, *90*, 041918.
- [15] M. Frentrup, L. Y. Lee, S.-L. Sahonta, M. J. Kappers, F. Massabuau, P. Gupta, R. A. Oliver, C. J. Humphreys, D. J. Wallis, *J. Phys. D: Appl. Phys.* **2017**, *50*, 433002.
- [16] W. Kong, H. Li, K. Qiao, Y. Kim, K. Lee, Y. Nie, D. Lee, T. Osadchy, R. J. Molnar, D. K. Gaskill, R. L. Myers-Ward, K. M. Daniels, Y. Zhang,

- S. Sundram, Y. Yu, S.-H. Bae, S. Rajan, Y. Shao-Horn, K. Cho, A. Ougazzaden, J. C. Grossman, J. Kim, *Nat. Mater.* **2018**, *17*, 999.
- [17] J. Mullay, in *Electronegativity* (Eds: K. D. Sen, C. K. Jørgensen), Springer-Verlag, Berlin/Heidelberg **1987**.
- [18] T. Schupp, K. Lischka, D. J. As, *J. Cryst. Growth* **2010**, *312*, 1500.
- [19] S. Hasegawa, in *Characterization of Materials* (Ed: E. N. Kaufmann), 2nd edition, Vol. 3, Wiley, Hoboken, NJ **2012**.
- [20] A. Ouerghi, A. Balan, C. Castelli, M. Picher, R. Belkhou, M. Eddrief, M. G. Silly, M. Marangolo, A. Shukla, F. Sirotti, *Appl. Phys. Lett.* **2012**, *101*, 021603.
- [21] A. Summerfield, A. Davies, T. S. Cheng, V. V. Korolkov, Y. Cho, C. J. Mellor, C. T. Foxon, A. N. Khlobystov, K. Watanabe, T. Taniguchi, L. Eaves, S. V. Novikov, P. H. Beton, *Sci. Rep.* **2016**, *6*, 22440.
- [22] Y. Goldberg, M. Levinshstein, S. Romyantsev, *SciTech Book News* **2001**, *6*, 22440.
- [23] M. Feneberg, M. Röppischer, C. Cobet, N. Esser, J. Schörmann, T. Schupp, D. J. As, F. Hörich, J. Bläsing, A. Krost, R. Goldhahn, *Phys. Rev. B* **2012**, *85*, 155207.
- [24] J. Lähnemann, U. Jahn, O. Brandt, T. Flissikowski, P. Dogan, H. T. Grahn, *J. Phys. D: Appl. Phys.* **2014**, *47*, 423001.